New Journal of Physics
The open access journal at the forefront of physics

Deutsche Physikalische Gesellschaft DPG
IOP Institute of Physics

Published in partnership with: Deutsche Physikalische Gesellschaft and the Institute of Physics

OPEN ACCESS

RECEIVED
15 September 2021

REVISED
16 November 2021

ACCEPTED FOR PUBLICATION
3 December 2021

PUBLISHED
29 December 2021

PAPER

Complexes formed in collisions between ultracold alkali-metal diatomic molecules and atoms

Matthew D Frye* and **Jeremy M Hutson***

Joint Quantum Centre (JQC) Durham-Newcastle, Department of Chemistry, Durham University, South Road, Durham DH1 3LE, United Kingdom

* Authors to whom any correspondence should be addressed.

E-mail: matthew.frye@durham.ac.uk and j.m.hutson@durham.ac.uk

Keywords: ultracold molecules, sticky collisions, ultracold scattering, Feshbach resonances

Abstract

We explore the properties of three-atom complexes of alkali-metal diatomic molecules with alkali-metal atoms, which may be formed in ultracold collisions. We estimate the densities of vibrational states at the energy of atom–diatom collisions, and find values ranging from 2.2 to 350 K^{-1}. However, this density does not account for electronic near-degeneracy or electron and nuclear spins. We consider the fine and hyperfine structure expected for such complexes. The Fermi contact interaction between electron and nuclear spins can cause spin exchange between atomic and molecular spins. It can drive inelastic collisions, with resonances of three distinct types, each with a characteristic width and peak height in the inelastic rate coefficient. Some of these resonances are broad enough to overlap and produce a background loss rate that is approximately proportional to the number of outgoing inelastic channels. Spin exchange can increase the density of states from which laser-induced loss may occur.

1. Introduction

Ultracold polar molecules have many potential applications, ranging from precision measurement [1–11], quantum simulation [12–17] and quantum information processing [18–24] to state-resolved chemistry [25–30]. A few molecules such as SrF [31–34], YO [35], CaF [36–38], YbF [39] and SrOH [40] have nearly closed vibronic transitions suitable for laser cooling. In addition, a variety of polar alkali-metal diatomic molecules have been produced by association of pairs of ultracold atoms, usually by magnetoassociation, followed by coherent optical transfer to the ground rovibronic state. The molecules produced in this way include KRb [41, 42], Cs_2 [43, 44], Rb_2 [45], RbCs [46, 47], NaK [48–50], NaRb [51], NaLi [52] and NaCs [53].

All the alkali-metal diatomic molecules produced so far have been found to undergo collisional loss in optical traps [27, 42, 46, 48, 51, 54], even in cases where there is no energetically allowed two-body reaction. In most systems the loss rate coefficients approach the predictions of a 'universal loss' model [55, 56] in which every molecular pair that reaches short range is lost from the trap. For RbCs, however, detailed loss measurements that include temperature dependence [54] have been used to determine the parameters of a non-universal model [57] in which there is partial reflection at short range.

Mayle *et al* [58, 59] proposed that the observed trap loss is due to 'sticky collisions', in which an initial bimolecular collision forms a long-lived complex that survives long enough to collide with a third molecule. They estimated the densities of states ρ for the four-atom complexes at the energy of the colliding molecules, and used arguments based on random-matrix theory (RMT) to estimate the resulting mean lifetime τ of the complex. For $(KRb)_2$ they obtained $\rho > 3000\ \mu K^{-1}$ and $\tau > 150$ ms. In subsequent work, Christianen *et al* [60] obtained improved estimates of ρ, taking fuller account of angular momentum constraints and using a more accurate representation of the potential energy surface. The corresponding lifetimes, $\tau = 6\ \mu s$ for $(NaK)_2$, are too short for most complexes to collide with a third molecule at the

experimental densities. Christianen *et al* [61] proposed that the complexes are instead excited by the trapping laser, and showed that this can occur fast enough to account for the observed trap loss. This proposal is supported by experiments on collisions of RbCs [62, 63] and ^{40}KRb [64], though recent experiments on Na^{40}K [65] and on Na^{39}K and Na^{87}Rb [66] suggest that the complexes have longer lifetimes than predicted in the absence of the trapping laser.

In parallel with the work on molecule-molecule collisions, experiments have been carried out on atom–molecule collisions. The systems studied experimentally include ^{40}K^{87}Rb with ^{40}K and ^{87}Rb [27, 67], ^{87}RbCs with ^{87}Rb and Cs [63], Na^{39}K with Na and ^{39}K [42, 68] and Na^{40}K with ^{40}K [50, 69]. For each molecule, reaction is energetically allowed in a collision with the lighter atom but forbidden in a collision with the heavier one. Fast collisional loss has been observed in all cases where the reaction is energetically allowed.

For non-reactive atom–molecule systems, the picture is more complicated. Experiments have been carried out on a number of systems including ^{40}K^{87}Rb with ^{87}Rb [27, 67], ^{87}RbCs with Cs [63], Na^{39}K with ^{39}K [42, 68] and Na^{40}K with ^{40}K [50]. For the last of these, Yang *et al* [50] observed narrow Feshbach resonances as a function of magnetic field; these resonances have been assigned as due to long-range states of triatomic complexes [69]. A wide variety of behaviour has been observed, ranging from near-universal loss to very slow loss, and no consistent picture is yet available. Recently, Nichols *et al* [67] directly probed complexes in collisions of ^{40}K^{87}Rb with ^{87}Rb; they measured lifetimes of 0.4 ms in the absence of the trapping laser, 5 orders of magnitude larger than theoretical predictions [60].

The purpose of the present paper is to explore the properties of the collision complexes that can be formed in collisions between alkali-metal diatomic molecules and atoms. The structure of the paper is as follows. In section 2, we consider the angular momenta that are present in alkali-metal triatomic systems, and basic aspects of the coupling between them. In section 3, we consider the relationship between densities of states, lifetimes of complexes, and loss rates, including threshold effects. In section 4, we estimate the densities of vibrational states for short-range three-atom complexes near the atom–diatom collision threshold. In section 5 we consider the electronic structure of the complexes and the effect of orbital near-degeneracy. In section 6, we present a model for the Fermi contact interaction between electron and nuclear spins, and show that it can drive spin exchange between atomic and molecular spins. In section 7, we consider the effect of spin exchange in atom-molecule collisions. We show that it can cause Feshbach resonances of three distinct types, each of which produces peaks in the loss rate coefficient with characteristic widths and peak heights. Some of these resonances are broad enough to overlap and produce a background loss rate that is approximately proportional to the number of outgoing inelastic channels. Finally, section 8 presents perspectives and conclusions of the work.

2. Angular momentum coupling

There are 6 sources of angular momentum in a triatomic system AB + C formed from a singlet molecule and an alkali-metal atom: the electron spin $S = 1/2$, three nuclear spins i_A, i_B, i_C, the diatomic rotation n and the partial-wave quantum number L for rotation of AB and C about one another.

An atom–diatom system in a single electronic state is governed by a three-dimensional potential energy surface $V(R, r, \theta)$. This is written here in Jacobi coordinates where r is the diatom bond length and R and θ are the atom–diatom distance and angle. For the alkali-metal systems of interest here, $V(R, r, \theta)$ is deep (of order 50 THz) and provides strong coupling between the vibrational and rotational states of the diatomic molecule. Nevertheless, it is diagonal in the total spin-free angular momentum N, which is the resultant of n and L.

An alkali-metal atom C in a ^{2}S state, with electron spin $S = 1/2$ and nuclear spin i_C, is characterized in zero field by its total spin $f_C = i_C \pm \frac{1}{2}$. The two hyperfine states are separated by the hyperfine splitting $(i_C + \frac{1}{2})\zeta_C$, of order 1 GHz, where ζ_C is the scalar hyperfine coupling constant that arises from the Fermi contact interaction. In a magnetic field, each hyperfine state is split into $2f_C + 1$ Zeeman states labeled by $m_{f,C}$. As will be seen below, the Fermi contact interaction in a triatomic complex can depend strongly on geometry and provides a coupling that can be off-diagonal in f_C and/or $m_{f,C}$, while conserving the total spin projection $m_{f,tot} = m_A + m_B + m_C + M_S$.

Our overall picture of the states of the triatomic complex is that the electronic interaction potential creates a strongly coupled and potentially chaotic manifold of states for each spin combination $(m_A, m_B, f_C, m_{f,C})$, which correlates at long range with an atom in state $(f_C, m_{f,C})$ and a molecule in state (m_A, m_B). There is a weaker coupling between manifolds of the same $m_{f,tot}$, due to the Fermi contact interaction, that may cause inelastic loss when there are suitable open channels.

Both the electronic interaction potential and the Fermi contact interaction conserve the total spin-free angular momentum N and its projection M_N. There are weaker interactions arising from Zeeman,

spin-rotation, and additional hyperfine interactions, some of which are off-diagonal in N and M_N. These may play a role in sharp Feshbach resonances, but are unlikely to be strong enough to influence background loss.

Atom–molecule pairs that reach short range may be excited by the trapping laser, producing laser-induced loss analogous to that observed in molecule–molecule collisions. This is possible both for direct collisions and for collisions that form long-lived complex; laser-induced loss is not in itself evidence of complex formation.

3. Resonance widths and lifetimes of collision complexes

A quasibound state is often thought of as characterized by a width Γ and a corresponding lifetime $\tau = \hbar/\Gamma$. However, these quantities need careful definition. When a bound state is embedded in a scattering continuum, it produces a resonance whose width Γ is governed by the matrix elements between the bound state and the continuum. If the state is well above the threshold of a single open channel, the scattering phase shift $\delta(E)$ follows the Breit–Wigner form,

$$\delta(E) = \delta_{\rm bg} + \arctan\left(\frac{\Gamma}{2(E_0 - E)}\right), \tag{1}$$

where $\delta_{\rm bg}$ is the background phase shift and E_0 is the resonance energy. If there are several open channels a, the S-matrix eigenphase sum [70] follows the form (1) and Γ is a sum of partial widths Γ_a to the individual open channels.

When a quasibound state is probed by absorption spectroscopy with a narrow-band laser from a single initial state, and the continuum itself is dark, the spectrum has a Lorentzian lineshape with width Γ [71–73]. Conversely, excitation of the entire Lorentzian, by a laser that is broad compared to Γ, produces a non-stationary state (wavepacket) that decays into the continuum with lifetime $\tau = \hbar/\Gamma$ [74]. Nevertheless, it is important to realize that, even when a bound state is spread out over a continuum, solutions of the time-independent Schrödinger equation still exist at each energy. Such solutions represent stationary states whose densities do not evolve in time. The rate at which a wavepacket can evolve is ultimately limited by its spread in energy, which can be much smaller than Γ. This is particularly important in ultracold systems, which may possess a very small energy spread characterized by their temperature. Complexes formed in ultracold systems may thus exhibit lifetimes limited by the temperature, which may be much longer than implied by the width of the underlying state.

The width of a Feshbach resonance is energy-dependent when the state lies just above threshold, even if the underlying couplings are independent of energy. In quantum defect theory (QDT), the partial width for decay of a resonance to an open channel a is

$$\Gamma_a = \Gamma_a^{\rm s} C^{-2}(E_a), \tag{2}$$

where $\Gamma_a^{\rm s}$ is the short-range width and $C^{-2}(E_a)$ is a QDT function that depends on the kinetic energy E_a for channel a [75–78]. For an interaction potential $-C_6R^{-6}$, $C^{-2}(E_a)$ depends on the background scattering length $a_{\rm bg}$ and is a universal function when written in terms of the mean scattering length $\bar{a} = (2\mu C_6/\hbar^2)^{1/4} \times 0.477\,988\,8\ldots$ [79] and the corresponding energy $\bar{E} = \hbar^2/(2\,\mu\bar{a}^2)$. Examples of $C^{-2}(E_a)$ are shown for a variety of values of $a_{\rm bg}/\bar{a}$ in figure 1; it is proportional to $E_a^{1/2}$ at limitingly low energy and in all cases it approaches 1 when $E_a \gg \bar{E}$. Because of this, $\Gamma_a \ll \Gamma_a^{\rm s}$ near threshold.

For molecules with regular patterns of energy levels, such as most low-lying vibrational states, the widths are unrelated to the spacings between levels and are often much smaller than them. However, Mayle *et al* [58, 59] suggested that the vibrational states of an atom–molecule or molecule–molecule collision complex are chaotic in nature, and may be approximated by RMT. Under these circumstances the mean short-range width of the states may be written in terms of their mean spacing d [80],

$$\bar{\Gamma}_a^{\rm s} = \frac{T_a^{\rm s} d}{2\pi}, \tag{3}$$

where $T_a^{\rm s}$ is a transmission coefficient between 0 and 1 that governs the likelihood of complex formation or decay for collisions that reach short range in channel a. Neglecting threshold effects, it is related to the unitarity deficit of the mean S matrix $\bar{S}$ by $T_a^{\rm s} = 1 - |\bar{S}_{aa}|^2$ [80].

Mayle *et al* [58, 59] gave estimates of lifetimes for collision complexes in atom–molecule and molecule–molecule collisions based on $\bar{\tau} = \hbar/\bar{\Gamma}$ and further estimated $\bar{\Gamma}$ as $d/(2\pi)$ to obtain the mean lifetime as $\bar{\tau} = 2\pi\hbar\rho$. Christianen *et al* [60] obtained better estimates for ρ but used the same procedure to estimate $\bar{\tau}$. However, this neglects the reduction of Γ both by threshold effects and by the short-range

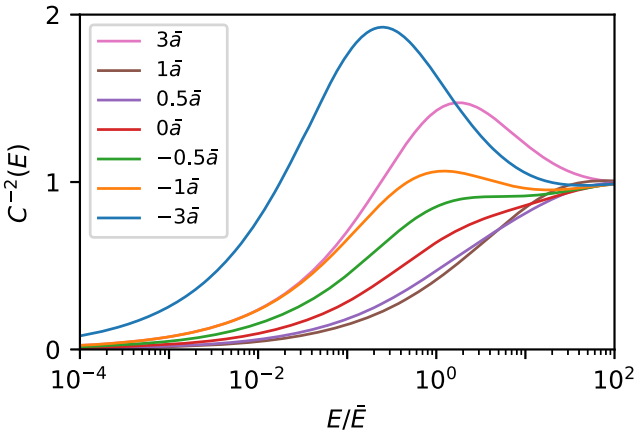

Figure 1. QDT parameter $C^{-2}(E)$ as a function of reduced energy $E/\bar{E}$ for a selection of background scattering lengths $a_{\rm bg}$.

transmission coefficient $T_a^{\rm s}$. The actual widths of the resonances are thus likely to be considerably smaller than the estimates of Mayle *et al*, and the lifetimes of the complexes, once formed, are likely to be considerably larger than $\tau = 2\pi\hbar\rho$. In general, if the temperature T is high enough to average over many resonances, $k_{\rm B}T \gg d$, then $\bar{\tau} = 2\pi\hbar\rho$ is still the correct mean collisional time delay [81], but only a fraction of collisions form complexes and those that do have extended lifetimes.

The effects of thresholds and of $T_a^{\rm s}$ can be combined into a single transmission coefficient T_a, which is generally not a simple product of the two contributions. In the presence of partial reflection at short range, T_a can be calculated from a non-universal QDT theory [55, 57]. The formation of complexes, averaged over many resonances, can be described in the same way as inelastic loss [82] and characterized by a short-range parameter analogous to the loss parameter y of Idziaszek and Julienne [55], where $T_a^{\rm s} = 4y/(1+y^2)$ [80]. The collision complex may subsequently decay back to the incoming channel, or be lost by a secondary process such as collision with a 3rd body, laser excitation, or inelastic decay. If the system behaves chaotically, the mean width for decay back to the incoming channel is $\bar{\Gamma}_{\rm inc} = T_{\rm inc}d/(2\pi)$. In the absence of other loss processes, this implies a mean lifetime $\bar{\tau} = 2\pi\hbar\rho/T_{\rm inc}$, but only if the thermal energy spread is large compared to $\bar{\Gamma}_{\rm inc}$ as described above. Christianen *et al* [83] recently considered a lossy QDT model of such resonances. They concluded that if the complexes are lost rapidly once formed and $\bar{\Gamma}^{\rm s}_{\rm inc} = d/2\pi$, such that $T^{\rm s}_{\rm inc} = 1$ in equation (3), the loss rate is represented by $y = 0.25$, as opposed to the $y = 1$ implicit in the model of Croft *et al* [82]. The reasons for this apparent disagreement are not clear at present, but both methods rely on averaging over a large number of resonances.

The densities of states for atom–molecule collision complexes are much lower than those for molecule–molecule complexes [60]. In particular, as seen below, the mean spacings between levels are far larger than both typical thermal energies and laser broadening. It is therefore not appropriate to average across the resonance widths. Instead, we need to consider how the possible presence of a single resonant state near threshold can enhance collisional loss. In the following, we consider this in terms of the resonant profile as the state crosses the incoming threshold, even if its energy relative to threshold is almost fixed. As shown in the appendix, the rate coefficient for resonant inelastic loss due to a single resonance with no background loss, at limitingly low collision energy, shows a Lorentzian peak of the form

$$k_2 = k_2^{\rm univ}\left[1 + \left(1 - a_{\rm bg}/\bar{a}\right)^2\right]\frac{\Gamma^{\rm s}_{\rm inc}/\Gamma_{\rm inel}}{[2(E-E_{\rm res})/\Gamma_{\rm inel}]^2 + 1}. \tag{4}$$

Here $k_2^{\rm univ} = 4\pi\hbar\bar{a}/\mu$ is the universal rate coefficient at zero energy [55]; values of $\bar{a}$ and $k_2^{\rm univ}$ are given in table 1. $\Gamma^{\rm s}_{\rm inc}$ is the short-range partial width for decay to the incoming channel, which may be well represented by equation (3). $\Gamma_{\rm inel}$ is the sum of the partial widths for secondary loss processes, including both laser excitation and inelastic decay. The width of the peak is determined by $\Gamma_{\rm inel}$, which is not subject to threshold effects in the incoming channel. It is entirely possible for the resonantly enhanced loss rate to exceed the universal rate, particularly when $\Gamma^{\rm s}_{\rm inc} > \Gamma_{\rm inel}$. Such supra-universal rates are observed, for example, near Feshbach resonances for $Na^{40}K$ with ^{40}K [50].

If $\Gamma_{\rm inel} \gtrsim d$, which often occurs when there are many open channels, multiple resonant features may overlap. When only a few resonances overlap, the separate contributions may be approximately additive. However, when many resonances overlap, they reach the regime of Ericson fluctuations [80] and the total

Table 1. Properties of atom + diatom systems: mean scattering length $\bar{a}$ and zero-temperature universal rate constant $k_2^{\rm univ}$, together with densities of short-range states ρ and mean spacings d calculated from equations (5) and (7).

System	$\bar{a}$ (Å)	$\bar{E}/h$ (MHz)	$k_2^{\rm univ}$ (cm^3 s^{-1})	$k_{\rm B}\rho(D_{\rm e})$ (K^{-1})	d/h (MHz)
^{7}Li^{7}Li + ^{7}Li	21	245	3.58×10^{-10}	2.2	9480
^{7}Li^{23}Na + ^{7}Li	20.8	205	2.92×10^{-10}	3.87	5386
^{7}Li^{40}K + ^{7}Li	23.2	154	3.03×10^{-10}	5.92	3520
^{7}Li^{87}Rb + ^{7}Li	24.2	132	2.96×10^{-10}	7.31	2852
^{7}Li^{133}Cs + ^{7}Li	25.4	117	3.04×10^{-10}	9.36	2225
^{7}Li^{23}Na + ^{23}Na	26	57.3	1.6×10^{-10}	4.61	4520
^{23}Na^{23}Na + ^{23}Na	29	39.1	1.51×10^{-10}	9.49	2195
^{23}Na^{40}K + ^{23}Na	30.8	31.6	1.46×10^{-10}	18.6	1122
^{23}Na^{87}Rb + ^{23}Na	32.5	25.1	1.37×10^{-10}	26.7	779
^{23}Na^{133}Cs + ^{23}Na	34.3	21.4	1.37×10^{-10}	37.8	551
^{7}Li^{40}K + ^{40}K	36.2	17.8	1.34×10^{-10}	8.17	2549
^{23}Na^{40}K + ^{40}K	38	14.3	1.24×10^{-10}	20.6	1011
^{40}K^{40}K + ^{40}K	42	10.8	1.26×10^{-10}	37.3	559
^{40}K^{87}Rb + ^{40}K	42.9	9.05	1.13×10^{-10}	56.6	368
^{40}K^{133}Cs + ^{40}K	45	7.69	1.11×10^{-10}	77.9	267
^{7}Li^{87}Rb + ^{87}Rb	45.7	5.36	8.08×10^{-11}	14.6	1423
^{23}Na^{87}Rb + ^{87}Rb	47.3	4.66	7.77×10^{-11}	41.8	499
^{40}K^{87}Rb + ^{87}Rb	50.1	3.91	7.75×10^{-11}	75.5	276
^{87}Rb^{87}Rb + ^{87}Rb	53.4	3.06	7.35×10^{-11}	134	155
^{87}Rb^{133}Cs + ^{87}Rb	55	2.68	7.05×10^{-11}	200	104
^{7}Li^{133}Cs + ^{133}Cs	55.7	2.39	6.52×10^{-11}	26.4	790
^{23}Na^{133}Cs + ^{133}Cs	57	2.17	6.34×10^{-11}	76.2	273
^{40}K^{133}Cs + ^{133}Cs	59.6	1.89	6.33×10^{-11}	129	161
^{87}Rb^{133}Cs + ^{133}Cs	61.9	1.59	5.96×10^{-11}	240	86.7
^{133}Cs^{133}Cs + ^{133}Cs	65.2	1.34	5.88×10^{-11}	344	60.5

loss cannot be represented in this way. This situation has been considered by Christianen *et al* [83]. Here we will consider only the case $\Gamma_{\rm inel} < d$, which is applicable to typical alkali atom + diatom collisions.

4. Densities of states for collision complexes

The densities of states are much lower for three-atom than for four-atom complexes. Christianen *et al* [60] have developed a procedure for evaluating the density of states, based on a semiclassical phase-space integral incorporating angular momentum constraints. They obtain

$$\rho(E) = \frac{g_{NJp} 4\sqrt{2}\pi m_{\rm A} m_{\rm B} m_{\rm C}}{h^3(m_{\rm A}+m_{\rm B}+m_{\rm C})} \int^{V<E} \frac{Rr}{\sqrt{\mu R^2 + \mu_{\rm AB} r^2}} [E - V(R,r,\theta)]^{1/2} R^2 \, {\rm d}R \, r^2 \, {\rm d}r \, \sin\theta \, {\rm d}\theta. \tag{5}$$

Here g_{NJp} is a parity factor that accounts for the absence of a conserved parity in classical phase space, which is 1 for the systems considered here; m_X is the mass of atom X; $\mu_{\rm AB} = m_{\rm A} m_{\rm B}/(m_{\rm A}+m_{\rm B})$ is the reduced mass of the diatomic molecule AB; and $\mu = (m_{\rm A}+m_{\rm B})m_{\rm C}/(m_{\rm A}+m_{\rm B}+m_{\rm C})$ is the atom–diatom reduced mass. Christianen *et al* [60] included a degeneracy factor $g_{\rm ABC}$ in this expression to account for equivalent nuclei, but here we take that into account in considering hyperfine states below. The resulting density of vibrational states $\rho(E)$ is for a single electronic state and a single value of the spin-free total angular momentum N and its projection M_N.[1] It also neglects fine and hyperfine structure.

Equation (5) can be integrated numerically if a full interaction potential $V(R,r,\theta)$ is available. However, if we make some approximations we can obtain analytic expressions. We wish to estimate the density of states that are strongly enough coupled to form a chaotic bath. Such states exist principally at short range. We therefore fix the first term in the integrand to its value at the equilibrium geometry, $R = R_{\rm e}$ and $r = r_{\rm e}$. We also approximate the potential to be isotropic and harmonic around the minimum,

$$V(R,r,\theta) = \frac{1}{2}k_r(r-r_{\rm e})^2 + \frac{1}{2}k_R(R-R_{\rm e})^2. \tag{6}$$

[1] We adopt the usual spectroscopic notation for a molecule with spin, retaining J for the angular momentum including electron spin and F for the angular momentum including electron and nuclear spins. We retain upper-case letters for quantum numbers of the triatomic system, and use lower-case letters for quantum numbers that refer to individual colliding species.

The integral can now be evaluated analytically, giving

$$\int [E - V(R, r, \theta)]^{1/2} R^2 \, \mathrm{d}R \, r^2 \, \mathrm{d}r \, \sin\theta \, \mathrm{d}\theta = \frac{8\pi^2 E^{3/2}}{3\sqrt{k_r k_R}}. \tag{7}$$

Here the energy is relative to the potential minimum, and for the present purpose we evaluate ρ at $E = D_e$, the energy of the separated atom and diatomic molecule with respect to the energy of the triatomic minimum. We therefore conclude that the density of short-range states around the atom–diatom threshold is likely to scale approximately as

$$\frac{m_A m_B m_C}{(m_A + m_B + m_C)} \frac{R_e r_e}{\sqrt{\mu R_e^2 + \mu_{AB} r_e^2}} \frac{D_e^{3/2}}{\sqrt{k_r k_R}}. \tag{8}$$

The equilibrium geometries and binding energies D_e for all the alkali-metal three-atom systems containing 2 or 3 identical atoms have been obtained from electronic structure calculations [84]. For each system, we estimate the force constant k_R for the atom–diatom vibrations assuming a Lennard-Jones potential in R. This gives $k_R = 72 D_e/R_e^2$, where D_e is the binding energy of the trimer with respect to the atom + diatom threshold and $R_e = (C_6/D_e)^{1/6}$; for $XY + X$ systems we use C_6 coefficients from [85] and for $X + X_2$ systems we use twice the C_6 coefficient for $X + X$ [86]. The force constant k_r is taken to be the same as that determined for the free diatomic molecule XY from electronic spectroscopy [87–114]. The resulting densities of short-range states ρ and mean level spacings d for the systems considered here are given in table 1. We have selected one representative isotope of each element, and the small variations due to isotopic substitution can be calculated from equation (8) if needed. The values range from 60.5 MHz for $Cs_2 + Cs$ to 9.48 GHz for $Li_2 + Li$. Most of the differences come from the atomic and reduced masses, which vary by up to a factor of 20 between systems. The value obtained by this method for $K_2 + Rb$ is within 25% of that obtained by Christianen *et al* [60] by evaluating equation (5) using a different model potential.

5. Orbital near-degeneracy

To understand the chemical bonding in the collision complexes, it is useful first to consider the homonuclear alkali-metal triatomic molecules [115]. At a geometry corresponding to an equilateral triangle (point group D_{3h}), these systems are orbitally degenerate, with a single electron in an orbital of symmetry e'. The resulting state has symmetry ^{2}E, so is subject to a Jahn–Teller distortion; the actual equilibrium geometry is an obtuse isosceles triangle (point group C_{2v}). At this geometry the ground state has $^2B_2$ symmetry, but there is a low-lying excited state of $^2A_1$ symmetry. At lower-symmetry geometries the two states are mixed. The two resulting surfaces intersect along seams of conical intersections that include one at equilateral geometries. The three equivalent potential minima on the lower surface are connected by low-energy pathways through scalene and acute isosceles geometries; motion along these pathways gives rise to the phenomenon known as pseudorotation, with characteristic energy-level patterns.

For heteronuclear three-atom systems X_2Y, the situation is more complicated [84]. Some systems have ground states of $^2B_2$ symmetry with minima at isosceles geometries, while others have ground states of $^2A'$ symmetry at scalene geometries (point group C_s). Nevertheless, the principle remains that there are two electronic states of similar well depth that cross and avoided-cross as a function of nuclear coordinates. The resulting short-range states are strongly coupled to one another, so the near-degeneracy of the partially filled orbitals produces almost a doubling in the densities of states from the values of section 4.

6. The Fermi contact interaction

The strongest hyperfine term for both the free atom and the triatomic collision complex is the Fermi contact interaction. At long range this couples S to i_C for the free atom to form f_C. At short range, however, all three nuclei experience significant spin densities and S couples to all of i_A, i_B and i_C to give resultant f_{tot}. The coupling is of the form

$$\sum_{X=A,B,C} \zeta_X(R, \theta, \phi) \hat{\boldsymbol{i}}_X \cdot \hat{\mathbf{S}}, \tag{9}$$

where $\hat{\mathbf{S}}$ and $\hat{\boldsymbol{i}}_X$ are the operators for the electron and nuclear spin angular momenta. The coupling coefficients ζ_X are proportional to the product of the corresponding nuclear magnetic moment and the electron spin density at nucleus X. The spin densities are strongly dependent on geometry; as any one nucleus is pulled away from the other two, the electron spin localizes on the separating atom, until the full

hyperfine coupling of the free atom is achieved as $R \to \infty$. However, in the strongly interacting region the spin density is distributed between the three atoms and shifts substantially from one atom to another as the complex vibrates. The spin density at the nucleus is sensitive only to the spin population in atomic s orbitals, and is reduced if population is transferred to p orbitals.

There is some controversy over the Fermi contact interactions in alkali-metal triatomics near their equilibrium geometries. For Na_3 [116] and K_3 [117], electron-spin resonance (ESR) studies of matrix-isolated species show that the s-orbital spin densities on the 3 atoms sum to around 0.9 at the equilibrium geometry of the $^2B_2$ state, with most of the density on the two equivalent atoms. For Li_3 [118] and Na_2Li [119] the distribution is similar, but the densities sum to only 0.69 and 0.78, respectively. The Li_3 result has been confirmed by a molecular-beam study [120]. These results accord with a physical picture in which relatively little spin density is located in p orbitals. However, a molecular-beam microwave study on Na_3 [121] suggests that the Fermi contact interactions are much smaller than the ESR spin densities imply, and this is supported by electronic structure calculations [122]. These details do not affect the basic physics discussed in the present paper: the important feature is that the spin densities shift substantially between atoms as a function of wide-amplitude motions.

We have modeled the spin densities using a valence-bond method. This is related to the London–Eyring–Polanyi–Sato (LEPS) [123–126] approach, which has been widely used for interaction potentials, including those of the alkali-metal triatomic molecules [127, 128]. In the LEPS approach, the two doublet surfaces are [123]

$$V^{\pm}(R_{\rm AB}, R_{\rm BC}, R_{\rm AC}) = J_{\rm AB} + J_{\rm BC} + J_{\rm AC} \pm \left[\frac{1}{2}(K_{\rm AB} - K_{\rm BC})^2(K_{\rm BC} - K_{\rm AC})^2(K_{\rm AC} - K_{\rm AB})^2\right]^{1/2}, \qquad (10)$$

where R_{XY} is the separation of atoms X and Y, and J_{XY} and K_{XY} are two-atom Coulomb and exchange integrals. Values of these integrals can be estimated from the potential curves for the corresponding two-atom systems by writing their singlet and triplet curves as

$$^{1,3}V_{XY}(R_{XY}) = J_{XY} \pm K_{XY}, \qquad (11)$$

with only the two-body singlet and triplet potentials [87–114] as input.

The London equation (10) [123] gives only the energies of the surfaces. However, Slater's derivation [129] of it allows calculation of the corresponding eigenfunctions and spin densities as well. The eigenfunctions are expressed as linear combinations of Slater determinants. Each determinant represents a configuration with one electron in the s orbital of each atom; for doublet states with $M_S = \frac{1}{2}$, two atoms have spin projection $m_s = \frac{1}{2}$ and one has projection $-\frac{1}{2}$. Remarkably, there are some atomic arrangements near isosceles geometries where one of the three configurations dominates. For such arrangements, the spin density on the isolated atom is actually dominated by $m_s = -\frac{1}{2}$, with the opposite sign to the overall spin. This is a result that is quite impossible for a spin-restricted Hartree–Fock wavefunction with an unpaired electron in a single molecular orbital.

In a magnetic field, the Fermi contact interaction can mediate spin exchange between the electron and nuclear spins (and indirectly among the nuclear spins) while conserving the total spin projection $m_{f,\rm tot}$. Each rovibrational state of the triatomic complex will split into $N_{\rm hf}$ spin sublevels. If the atomic and molecular states are spin-stretched, $m_{f,\rm tot} = \pm f_{\rm max}$, where $f_{\rm max} = S + i_{\rm A} + i_{\rm B} + i_{\rm C}$, only a single sublevel exists for each rovibrational state of the complex. However, the number of sublevels increases as $|m_{f,\rm tot}|$ decreases. Neglecting exchange symmetry, there are $N_{\rm hf} = 4$ sublevels for $f_{\rm max} - |m_{f,\rm tot}| = 1$; three of these have even exchange parity and one is odd. For larger deviations the numbers increase, and are easily evaluated, but depend on the specific values of the spins.

An example of the effect of shifting spin density is shown in figure 2. This shows the Fermi contact contribution to the hyperfine energy for the reaction $^{87}Rb + {}^{40}K^{87}Rb \to {}^{87}Rb_2 + {}^{40}K$ along a selected reaction path that includes a rearrangement by pseudorotation. It is obtained by diagonalizing the Fermi-contact Hamiltonian (9) at each geometry, with the coupling coefficients ζ_X calculated from the valence-bond model. The resulting hyperfine adiabats are shown for $m_{f,\rm tot} = -3/2$, which corresponds to the lowest hyperfine state of the reactants. In this case, $f_{\rm max} - |m_{f,\rm tot}| = 6$ and there are $N_{\rm hf} = 32$ hyperfine sublevels. At the center of the diagram, where there is substantial exchange of spin density, the levels are spread out across an energy range comparable to the atomic hyperfine splitting and their energies depend strongly on geometry. There are many avoided crossings with a variety of widths, particularly along the pseudorotation section of the path, that are likely to result in spin exchange.

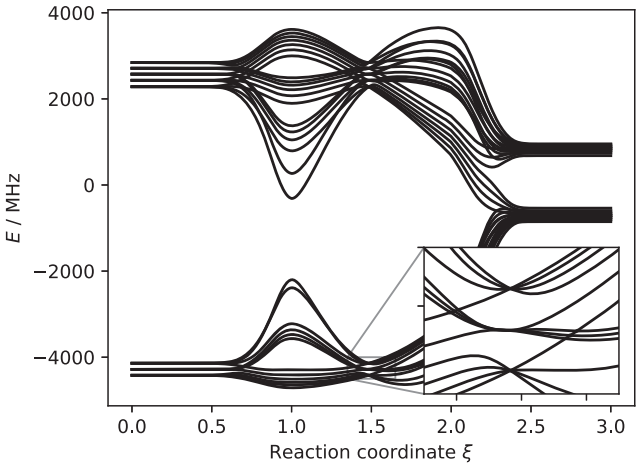

Figure 2. Energies of hyperfine adiabats of $^{87}Rb^{40}_2K$ with $m_{f,\mathrm{tot}} = -3/2$ in a magnetic field of 200 G, with spin densities taken from the valence-bond model. Along the coordinate ξ, the system starts from the separated Rb atom and KRb molecule ($\xi = 0$); these approach each other with fixed Rb–K–Rb angle, to the absolute minimum ($\xi = 1$), which is an obtuse isosceles triangle. The system then pseudorotates along the minimum-energy path to a local minimum at a scalene geometry ($\xi = 2$), and finally dissociates by moving the K atom away from Rb_2, with fixed Rb–Rb–K bond angle ($\xi = 3$). The inset shows an expansion of the adiabats around the midpoint of the pseudorotation, illustrating the presence of close avoided crossings that are likely to result in spin exchange.

7. Inelastic loss mediated by spin exchange

There is a manifold of short-range vibrational states associated with each hyperfine sublevel. Each such manifold is likely to be chaotic in nature. Spin exchange allows a collision between atoms and molecules in one pair of states to access bound states in any manifold with the same $m_{f,\mathrm{tot}}$. The density of states is enhanced to $N_{\mathrm{hf}}\rho$, and all the states can cause Feshbach resonances. However, these states are not necessarily equivalent, because the Fermi contact interaction that drives spin exchange is weaker than the anisotropic potential coupling. A given incoming channel couples strongly to one of these manifolds, but it may couple more weakly to the remaining $N_{\mathrm{hf}} - 1$ manifolds. This may be quantified with a spin-exchange parameter z, analogous to the isospin-mixing parameter used for reactions of compound nuclei [130],

$$z = \frac{4\pi^2\overline{H_{ab}^2}}{d^2}, \tag{12}$$

where H_{ab} is a matrix element of the coupling between states in manifolds a and b. When $z \ll 1$, the mean partial width connecting the incoming channel to states in these other manifolds is $z\bar{\Gamma}_a$. Conversely, when $z \gg 1$, states in the N_{hf} different manifolds are fully mixed and all contribute to the effective density of states that enters into RMT.

A full calculation of the spin-exchange parameter is beyond the scope of this work. It requires not only the mean level spacing d but also the wavefunctions of the states in the two chaotic manifolds. Such a calculation is near the limits of current theoretical methods, but may be achievable for lighter atom-diatom systems within a few years. Here we follow the practice in studies of compound nuclei [130], and treat z as a phenomenological parameter to be inferred from experimental results.

Spin exchange can also produce inelastic loss if there are channels lower in energy than the incoming state but with the same $m_{f,\mathrm{tot}}$. We again take $^{40}K^{87}Rb + {}^{87}Rb$ as our example [27, 67]. The lowest state of the separated atom and molecule is $(m_K, m_{Rb}, f_{Rb}, m_{f,Rb}) = (-4, 3/2, 1, 1)$. Excitation of either nuclear spin of the molecule individually does not produce any inelastic channels that are accessible by spin exchange, but the combined excitation to $(m_K, m_{Rb}) = (-3, 1/2)$ has the same $m_{f,\mathrm{tot}}$ as the ground state, so spin exchange is allowed. However, these two states states are split by only the nuclear Zeeman effect, so the kinetic energy release is small, equivalent to 15 μK at a representative magnetic field of 200 G. The corresponding QDT function $C^{-2}(E)$ is typically around 0.1, so decay by this path is partially suppressed by threshold effects. If the atom is in an excited state, spin exchange is usually energetically allowed. In such cases the kinetic energy releases are much larger, equivalent to 7 mK at 200 G, such that $C^{-2}(E)$ is close to 1, and loss is not suppressed by threshold effects.

Even when there are open channels that are energetically accessible, non-resonant spin exchange is likely to be slow. The avoided crossings in figure 2 occur deep in the potential well. Even for the widest such crossings, a Landau–Zener treatment estimates inelastic transition probabilities of the order of 10^{-3} for a

double crossing in Rb + KRb. Significant loss is therefore expected only when there is resonant enhancement. If $z < 1$, there are three general cases of resonant inelastic decay, which correspond to different values of $\Gamma^{\rm s}_{\rm inc}$ and $\Gamma_{\rm inel}$ in equation (4). In the following, we relate the mean heights of resonant loss features to the universal rate, modified by the factor $[1 + (1 - a_{\rm bg}/\bar{a})^2]$ in equation (4), and their mean widths to $\bar{\Gamma}^{\rm s}_a$ of equation (3).

The first case is where the resonant state is part of the manifold associated with the incoming channel and coupled to $N_{\rm out}$ inelastic channels by spin exchange. We refer to the resulting resonances as incoming-manifold resonances. The coupling to the incoming channel is characterized by $\bar{\Gamma}^{\rm s}_{\rm inc} = \bar{\Gamma}^{\rm s}_a$ and that to the inelastic channels by $\bar{\Gamma}_{\rm inel} = z\bar{\Gamma}^{\rm s}_a$. The height of the peak in the loss rate is thus multiplied by a factor $1/(zN_{\rm out})$, but its width is divided by the same factor. When it is appropriate to average over many such resonances, their total contribution is thus independent of z, but in the atom + molecule case, where the density of states is too low for averaging to be appropriate, the narrowing decreases the probability of hitting such a resonance.

The second case is where the resonant state is part of a manifold associated with an open channel other than the incoming channel. We refer to these as outgoing-manifold resonances. In this case $\bar{\Gamma}^{\rm s}_{\rm inc} = z\bar{\Gamma}^{\rm s}_a$ and $\bar{\Gamma}_{\rm inel} = \bar{\Gamma}^{\rm s}_a$. The height of the peak in loss rate is thus multiplied by a factor z. However the widths of the resonances are unaffected by z, so may be comparable to their spacings, according to equation (3). If there are $N_{\rm out}$ open channels, each of them will support resonances of this type.

The third case is where the resonant state is part of a manifold associated with a closed channel. We refer to these as closed-manifold resonances. In this case $\bar{\Gamma}^{\rm s}_{\rm inc} = z\bar{\Gamma}^{\rm s}_a$ and $\bar{\Gamma}_{\rm inel} = zN_{\rm out}\bar{\Gamma}^{\rm s}_a$. The height of the peak in loss rate is thus reduced by a factor $N_{\rm out}$ from the universal rate, and the width of the peak is multiplied by a factor $zN_{\rm out}$.

Figure 3 shows two schematic examples of the combined effect of these three types of resonance. For the purpose of illustration, we choose spin-exchange parameter $z = 0.15$ and short-range transmission coefficient $T^{\rm s}_a = 1.0$. For each manifold, the bound states are randomly generated from a suitable chaotic distribution[2] [131, 132] with mean spacing d. The horizontal axis represents scanning the energy of the incoming channel across the pattern of short-range bound states. The upper panel of figure 3 shows an example with $N_{\rm hf} = 9$ and $N_{\rm out} = 4$, so that within each interval d there is 1 incoming-manifold resonance, 4 outgoing-manifold resonances, and 4 closed-manifold resonances. It may be seen that the outgoing-manifold and closed-manifold resonances make similar overall contributions to the inelastic rate, but the closed-manifold contribution is more structured because the underlying resonances are narrower. The incoming-manifold resonances give peaks that are high but relatively narrow (with width dependent on $T^{\rm s}_a$), and usually will not overlap. The lower panel of figure 3 shows an example with $N_{\rm hf} = 9$ and $N_{\rm out} = 2$, with the resonances in the same locations as before to facilitate comparison. Within each interval d there are now 1, 2 and 7 incoming-, outgoing- and closed-manifold resonances, respectively. The major differences are that the peaks for incoming-manifold and closed-manifold resonances are higher and sharper, while the overall contribution of outgoing-channel resonances is reduced by the smaller $N_{\rm out}$. An important feature that the two examples share is a weakly structured background loss from the outgoing-manifold resonances, whose mean height is

$$k_2^{\rm bg} \approx \frac{zN_{\rm out}T^{\rm s}_a}{4} k_2^{\rm univ}, \tag{13}$$

independent of d.

The loss rates in figure 3 are shown as a function of the mean spacing d. In ultracold scattering, however, such rates are usually measured as a function of magnetic field, or some other external variable such as electric field. As a function of magnetic field B, channel thresholds shift with respect to one another by $B\Delta\mu$, where $\Delta\mu$ is the difference in magnetic moments. For free alkali-metal atoms at low field, $\Delta\mu/h \approx 1.4/(i_{\rm C} + \frac{1}{2})$ MHz G^{-1} for states with $m_{f,{\rm C}}$ that differ by 1, and is typically between 0.7 MHz G^{-1} for atoms with $i_{\rm C} = \frac{3}{2}$ (^{23}Na, ^{39}K, ^{41}K, ^{87}Rb) and 0.3 MHz G^{-1} for $i_{\rm C} = 4$ (^{40}K). The magnetic moments of triatomic complexes are more complicated, but will be of similar magnitude. The horizontal axes in figure 3 correspond to $3d$ and thus cover the equivalent of hundreds or even thousands of Gauss. The general conclusion is that atom-molecule resonances due to states that belong to the RMT bath are very broad indeed.

The largest body of experimental results for losses in alkali-metal atom–molecule systems is for Na^{40}K with ^{40}K. Yang *et al* [50] measured loss rates as a function of magnetic field for more than 20 combinations of atomic and molecular states. Their main focus was on narrow Feshbach resonances, but they also

[2] We randomly generate matrices of dimension 20 from the Gaussian orthogonal ensemble, and unfold the resulting eigenvalues analytically using Wigner's semicircle law.

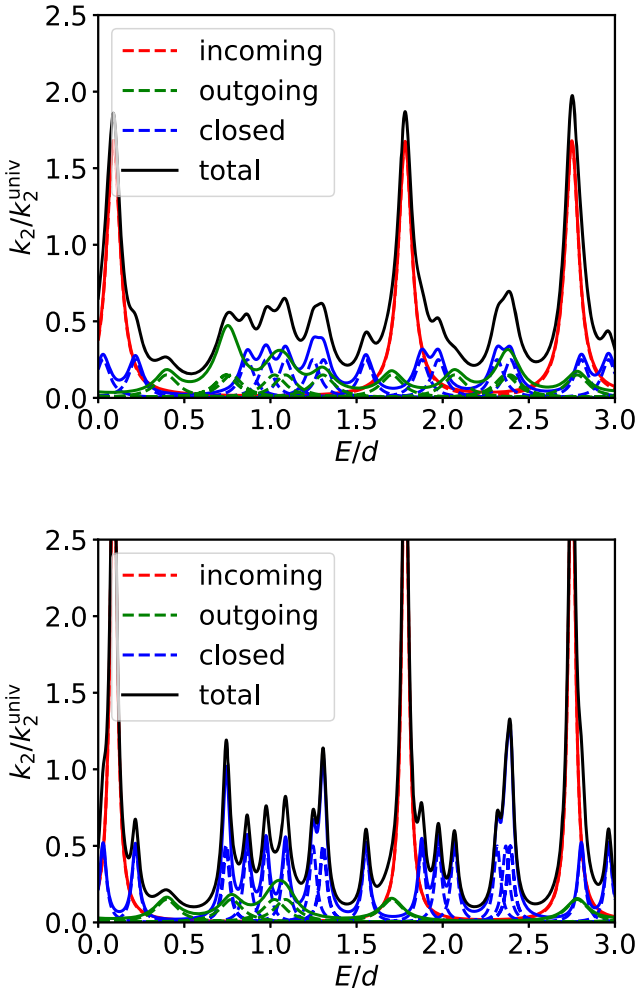

Figure 3. Schematic examples of loss due to the three types resonance. Red, green and blue lines show incoming-, outgoing-, and closed-manifold resonances, respectively; dashed lines show contributions of individual resonances from equation (4) and solid lines show simple sums neglecting interference effects. The coupling parameters used here are $T_a^{\rm s} = 1.0$ and $z = 0.15$. We choose $N_{\rm hf} = 9$, corresponding to $f_{\rm max} - |m_{f,\rm tot}| = 2$ for most alkali-metal trimer systems. The upper panel shows $N_{\rm out} = 4$ and the lower $N_{\rm out} = 2$.

measured loss rate coefficients in several windows of magnetic field, including near 90 G and near 102 G, shown in figures S2 and S3 of their supplemental material. In cases where no resonant features are visible, the background loss rates generally increase with $N_{\rm out}$, reaching values between 0.5 and 1 times the universal loss rate when $N_{\rm out}$ is 3 to 5. However, there are also a few state combinations that show unstructured loss at up to twice the universal rate. For Na^{40}K with ^{40}K, $d = 1033$ MHz and a typical value of $\Delta\mu/h$ is 0.3 MHz G^{-1}, so even the narrowest resonances in figure 3(b) have widths of order 200 G for $z = 0.15$. Both the general increase in background loss rates with $N_{\rm out}$ and the occasional state combinations with supra-universal rates are entirely consistent with the behaviour shown in figure 3.

In addition to inelastic loss to lower-lying open channels, there is the possibility of loss due to laser excitation of complexes by the trapping laser. This is likely to introduce loss from all channels accessible by spin exchange, with a contribution $\bar{\Gamma}_{\rm laser}$ to $\bar{\Gamma}_{\rm inel}$ that depends on the laser intensity but is independent of $\bar{\Gamma}_a^{\rm s}$ and hence of the density of states. The effect of this depends on the relative strength of this decay to any existing inelastic loss. Nichols *et al* [67] have measured decay equivalent to $\bar{\Gamma}_{\rm laser}/h \approx 5$ MHz for ^{40}KRb + Rb at typical optical trap intensities, and it seems likely that other alkali-metal atom + molecule systems will be comparable. This value is substantially smaller than our estimates of $\bar{\Gamma}_a^{\rm s}$ for any of the systems considered here. Laser-induced loss is thus likely to have little effect on loss due to any outgoing-manifold resonances, but it may reduce the height and increase the width of incoming-manifold or closed-manifold resonances if $\bar{\Gamma}_{\rm laser} \gtrsim z\bar{\Gamma}_a^{\rm s}$. More importantly, it may induce both incoming-manifold and closed-manifold resonances even in systems with no open inelastic channels, such as those involving atoms and molecules in their absolute ground states. However, the likelihood of encountering such a resonance for a particular incoming state at a single field is approximately $(N_{\rm hf} - 1)\bar{\Gamma}_{\rm laser}/d$, which is usually fairly small.

8. Conclusions

We have developed the theory of the triatomic complexes that can be formed in ultracold collisions between alkali-metal diatomic molecules and atoms. We have estimated the densities of vibrational states of the complexes near the energy of the colliding particles, based on the properties of the diatomic molecules and the calculated binding energies of the trimers. The resulting densities range from 2.2 to 350 K^{-1}. We have considered the angular momentum couplings present in the complexes and the resulting fine and hyperfine structure. The largest such term is the Fermi contact interaction between the electron and nuclear spins. We have presented a model of this interaction, based on valence-bond theory, and shown that it varies substantially with the geometry of the complex because the unpaired spin moves between the atoms as the complex vibrates.

Our overall picture is that each pair of atomic and molecular spin states is associated with a manifold of vibrational states of the triatomic complex. Each such manifold is likely to be chaotic in nature. The Fermi contact interaction can couple these manifolds, and can thus drive spin exchange between spins on the atom and the molecule. The degree of coupling between manifolds is characterized by a spin-exchange parameter z, which depends on the ratio between off-diagonal matrix elements of the Fermi contact interaction and the mean spacing between vibrational levels, d. This parameter may be substantial in the alkali-metal triatomic complexes.

We have developed the theory of resonant low-energy scattering in the presence of several chaotic manifolds that are weakly coupled to one another. We find that there can be Feshbach resonances of three distinct types, which we term incoming-, outgoing- and closed-manifold resonances. Each type of resonance can cause peaks in the rate coefficient for inelastic scattering with characteristic peak heights and widths that depend on z and the number of outgoing inelastic channels. For atom–diatom systems, the resonances due to states in the chaotic bath are very broad compared to the spread of kinetic energies at ultracold temperatures, so it is not appropriate to average over their widths in ultracold atom–diatom collisions. Instead, the scattering properties at a specific collision threshold depend on its energy with respect to the essentially random pattern of individual bath states. Nevertheless, the resonances due to outgoing-manifold resonances are broad enough that they may overlap to produce a background loss for most incoming states, particularly when there are several outgoing inelastic channels that are accessible from the incoming state by spin exchange.

Resonances due to states in the chaotic bath are different from those arising from near-threshold states of triatomic complexes, as observed in $Na^{40}K + {}^{40}K$ [69]. Such states spend most of their time in the long-range tail of the interaction potential; they are relatively weakly coupled to one another and to the incoming and outgoing scattering states, so they can produce much narrower resonances than the states considered here. They do not form part of the chaotic bath of states, so there is no reason to expect their widths to be related to their spacings.

Atom–diatom complexes have much lower densities of states than diatom–diatom complexes. Nevertheless, some features of the theory developed here may apply in the diatom–diatom case. In particular, the densities of states in diatom-diatom complexes [60] can be 4 orders of magnitude larger than those obtained here for atom–diatom complexes. Since the mixing between manifolds is governed by the *ratio* of couplings to level spacings, much smaller couplings are sufficient to cause mixing in the diatom–diatom case. Even very small interactions such as the nuclear electric quadrupole coupling [133] might be large enough.

Acknowledgments

This work was supported by the UK Engineering and Physical Sciences Research Council (EPSRC) Grant No. EP/P01058X/1.

Data availability statement

The data that support the findings of this study are openly available at the following URL/DOI: 10.15128/r2sb397829n.

Appendix A. Scattering length and loss rate across a decayed resonance

Hutson [134] has described the behaviour of a Feshbach resonance close to threshold in the presence of inelastic decay. The general expression for an S-matrix element in the vicinity of a resonance is

$$S_{ab}(E) = S_{\mathrm{bg},ab} - \frac{\mathrm{i}g_a g_b}{E - E_{\mathrm{res}} + \mathrm{i}\Gamma/2}. \tag{A.1}$$

Here, E_{res} is the resonance energy, g_a is in general complex and characterizes the partial width $\Gamma_a = |g_a^2|$, and $\Gamma = \sum_a \Gamma_a$ is the total width. We are interested in the diagonal S-matrix element in the incoming channel, S_{inc}; we take the collision energy $E - E_{\mathrm{inc}}$ to be small, such that we can approximate the background S-matrix element to be $S_{\mathrm{bg,inc}} = 1$; the more general case $|S_{\mathrm{bg,inc}}| = 1$ gives the same results for inelastic loss due to resonances, but we choose this specific value for simplicity. With this choice, the product g_{inc}^2 must be real and non-negative and can be replaced by Γ_{inc}, the partial width to the incoming channel. This gives

$$S_{\mathrm{inc}} = 1 - \frac{\mathrm{i}\Gamma_{\mathrm{inc}}}{(E - E_{\mathrm{res}}) + \mathrm{i}\Gamma/2}. \tag{A.2}$$

The total width is $\Gamma = \Gamma_{\mathrm{inc}} + \Gamma_{\mathrm{inel}}$, where Γ_{inel} characterizes the decay to all loss channels, whether inelastic, reactive, or light-induced. The partial width in the incoming channel is narrowed by threshold effects, $\Gamma_{\mathrm{inc}} = \Gamma_{\mathrm{inc}}^{\mathrm{s}} C^{-2}(E - E_{\mathrm{inc}})$, as described by equation (2).

The QDT function $C^{-2}(E_{\mathrm{kin}})$ can be calculated explicitly from either numerical or analytic solutions [135] with an appropriate asymptotic potential. Its leading term for an asymptotic potential $-C_6/R^6$ is [77, 78, 136]

$$C^{-2}(E_{\mathrm{kin}}) = k\bar{a}\left[1 + \left(1 - a_{\mathrm{bg}}/\bar{a}\right)^2\right], \tag{A.3}$$

where $k = \sqrt{2\,\mu E_{\mathrm{kin}}}/\hbar$ is the wavevector and a_{bg} is the background (non-resonant) scattering length.

We could now directly calculate inelastic cross sections and rate coefficients from equation (A.2), but it is convenient first to consider the complex scattering length. This is defined as [134]

$$\begin{aligned} a(k) &= \alpha - \mathrm{i}\beta \\ &= \frac{1}{\mathrm{i}k}\frac{1 - S_{\mathrm{inc}}}{1 + S_{\mathrm{inc}}} \end{aligned} \tag{A.4}$$

and the two-body loss rate coefficient is

$$k_2 = \frac{4\pi\hbar\beta}{\mu(1 + k^2|a|^2 + 2k\beta)}. \tag{A.5}$$

This becomes constant and proportional to β at low energy; the universal rate at zero energy, k_2^{univ} corresponds to $\beta = \bar{a}$ [55]. Substituting equation (A.2) into equation (A.4) and using equation (A.3) gives

$$a = \bar{a}\left[1 + \left(1 - a_{\mathrm{bg}}/\bar{a}\right)^2\right]\frac{\Gamma_{\mathrm{inc}}^{\mathrm{s}}/\Gamma_{\mathrm{inel}}}{2(E - E_{\mathrm{res}})/\Gamma_{\mathrm{inel}} + \mathrm{i}}, \tag{A.6}$$

and so

$$\beta = \bar{a}\left[1 + \left(1 - a_{\mathrm{bg}}/\bar{a}\right)^2\right]\frac{\Gamma_{\mathrm{inc}}^{\mathrm{s}}/\Gamma_{\mathrm{inel}}}{[2(E - E_{\mathrm{res}})/\Gamma_{\mathrm{inel}}]^2 + 1}. \tag{A.7}$$

This can be converted to a rate through equation (A.5). We make the simplifying assumption that $k|a| \ll 1$, such that the denominator in equation (A.5) reduces to just μ, and write the result in terms of $k_2^{\mathrm{univ}} = 4\pi\hbar\bar{a}/\mu$. This gives

$$k_2 = k_2^{\mathrm{univ}}\left[1 + \left(1 - a_{\mathrm{bg}}/\bar{a}\right)^2\right]\frac{\Gamma_{\mathrm{inc}}^{\mathrm{s}}/\Gamma_{\mathrm{inel}}}{[2(E - E_{\mathrm{res}})/\Gamma_{\mathrm{inel}}]^2 + 1}. \tag{A.8}$$

which is equation (4). This is a Lorentzian peak with width determined only by Γ_{inel}, and a peak height that reaches at least the universal rate if $\Gamma_{\mathrm{inc}}^{\mathrm{s}} \geqslant \Gamma_{\mathrm{inel}}$.

ORCID iDs

Matthew D Frye https://orcid.org/0000-0003-4807-2807
Jeremy M Hutson https://orcid.org/0000-0002-4344-6622

References

[1] Zelevinsky T, Kotochigova S and Ye J 2008 Precision test of mass-ratio variations with lattice-confined ultracold molecules *Phys. Rev. Lett.* **100** 043201
[2] Hudson J J, Kara D M, Smallman I J, Sauer B E, Tarbutt M R and Hinds E A 2011 Improved measurement of the shape of the electron *Nature* **473** 493
[3] Salumbides E J, Dickenson G D, Ivanov T I and Ubachs W 2011 QED effects in molecules: test on rotational quantum states of H_2 *Phys. Rev. Lett.* **107** 043005
[4] Salumbides E J, Koelemeij J C J, Komasa J, Pachucki K, Eikema K S E and Ubachs W 2013 Bounds on fifth forces from precision measurements on molecules *Phys. Rev.* D **87** 112008
[5] Schiller S, Bakalov D and Korobov V 2014 Simplest molecules as candidates for precise optical clocks *Phys. Rev. Lett.* **113** 023004
[6] Baron J *et al* (The ACME Collaboration) 2014 Order of magnitude smaller limit on the electric dipole moment of the electron *Science* **343** 269
[7] Hanneke D, Carollo R A and Lane D A 2016 High sensitivity to variation in the proton-to-electron mass ratio in O_2^+ *Phys. Rev.* A **94** 050101(R)
[8] Cairncross W B, Gresh D N, Grau M, Cossel K C, Roussy T S, Ni Y, Zhou Y, Ye J and Cornell E A 2017 Precision measurement of the electron's electric dipole moment using trapped molecular ions *Phys. Rev. Lett.* **119** 153001
[9] Borkowski M 2018 Optical lattice clocks with weakly bound molecules *Phys. Rev. Lett.* **120** 083202
[10] The ACME Collaboration 2018 Improved limit on the electric dipole moment of the electron *Nature* **562** 355
[11] Borkowski M, Buchachenko A A, Ciuryło R, Julienne P S, Yamada H, Kikuchi Y, Takasu Y and Takahashi Y 2019 Weakly bound molecules as sensors of new gravitylike forces *Sci. Rep.* **9** 14807
[12] Barnett R, Petrov D, Lukin M and Demler E 2006 Quantum magnetism with multicomponent dipolar molecules in an optical lattice *Phys. Rev. Lett.* **96** 190401
[13] Micheli A, Brennen G K and Zoller P 2006 A toolbox for lattice-spin models with polar molecules *Nat. Phys.* **2** 341
[14] Büchler H P, Demler E, Lukin M, Micheli A, Prokof'ev N, Pupillo G and Zoller P 2007 Strongly correlated 2D quantum phases with cold polar molecules: controlling the shape of the interaction potential *Phys. Rev. Lett.* **98** 060404
[15] Macià A, Hufnagl D, Mazzanti F, Boronat J and Zillich R E 2012 Excitations and stripe phase formation in a two-dimensional dipolar Bose gas with tilted polarization *Phys. Rev. Lett.* **109** 235307
[16] Manmana S R, Stoudenmire E M, Hazzard K R A, Rey A M and Gorshkov A V 2013 Topological phases in ultracold polar-molecule quantum magnets *Phys. Rev.* B **87** 081106(R)
[17] Gorshkov A V, Hazzard K R A and Rey A M 2013 Kitaev honeycomb and other exotic spin models with polar molecules *Mol. Phys.* **111** 1908
[18] DeMille D 2002 Quantum computation with trapped polar molecules *Phys. Rev. Lett.* **88** 067901
[19] Yelin S F, Kirby K and Côté R 2006 Schemes for robust quantum computation with polar molecules *Phys. Rev.* A **74** 050301(R)
[20] Zhu J, Kais S, Wei Q, Herschbach D and Friedrich B 2013 Implementation of quantum logic gates using polar molecules in pendular states *J. Chem. Phys.* **138** 024104
[21] Herrera F, Cao Y, Kais S and Whaley K B 2014 Infrared-dressed entanglement of cold open-shell polar molecules for universal matchgate quantum computing *New J. Phys.* **16** 075001
[22] Ni K-K, Rosenband T and Grimes D D 2018 Dipolar exchange quantum logic gate with polar molecules *Chem. Sci.* **9** 6830
[23] Sawant R, Blackmore J A, Gregory P D, Mur-Petit J, Jaksch D, Aldegunde J, Hutson J M, Tarbutt M R and Cornish S L 2020 Ultracold polar molecules as qudits *New J. Phys.* **22** 013027
[24] Hughes M *et al* 2020 Robust entangling gate for polar molecules using magnetic and microwave fields *Phys. Rev.* A **101** 062308
[25] Krems R V 2008 Cold controlled chemistry *Phys. Chem. Chem. Phys.* **10** 4079
[26] Bell M T and Softley T P 2009 Ultracold molecules and ultracold chemistry *Mol. Phys.* **107** 99
[27] Ospelkaus S *et al* 2010 Quantum-state controlled chemical reactions of ultracold KRb molecules *Science* **327** 853
[28] Dulieu O, Krems R, Weidemüller M and Willitsch S 2011 Physics and chemistry of cold molecules *Phys. Chem. Chem. Phys.* **13** 18703
[29] Balakrishnan N 2016 Perspective: ultracold molecules and the dawn of cold controlled chemistry *J. Chem. Phys.* **145** 150901
[30] Hu M-G *et al* 2019 Direct observation of bimolecular reactions of ultracold KRb molecules *Science* **366** 1111
[31] Shuman E S, Barry J F and DeMille D 2010 Laser cooling of a diatomic molecule *Nature* **467** 820
[32] Barry J F, McCarron D J, Norrgard E B, Steinecker M H and DeMille D 2014 Magneto-optical trapping of a diatomic molecule *Nature* **512** 286
[33] McCarron D J, Norrgard E B, Steinecker M H and DeMille D 2015 Improved magneto-optical trapping of a diatomic molecule *New J. Phys.* **17** 035014
[34] Norrgard E B, McCarron D J, Steinecker M H, Tarbutt M R and DeMille D 2016 Submillikelvin dipolar molecules in a radio-frequency magneto-optical trap *Phys. Rev. Lett.* **116** 063004
[35] Hummon M T, Yeo M, Stuhl B K, Collopy A L, Xia Y and Ye J 2013 2D magneto-optical trapping of diatomic molecules *Phys. Rev. Lett.* **110** 143001
[36] Zhelyazkova V, Cournol A, Wall T E, Matsushima A, Hudson J J, Hinds E A, Tarbutt M R and Sauer B E 2014 Laser cooling and slowing of CaF molecules *Phys. Rev.* A **89** 053416
[37] Truppe S, Williams H J, Hambach M, Caldwell L, Fitch N J, Hinds E A, Sauer B E and Tarbutt M R 2017 Molecules cooled below the Doppler limit *Nat. Phys.* **13** 1173
[38] Anderegg L, Augenbraun B L, Bao Y, Burchesky S, Cheuk L W, Ketterle W and Doyle J M 2018 Laser cooling of optically trapped molecules *Nat. Phys.* **14** 890
[39] Lim J, Almond J R, Trigatzis M A, Devlin J A, Fitch N J, Sauer B E, Tarbutt M R and Hinds E A 2018 Laser cooled YbF molecules for measuring the electron's electric dipole moment *Phys. Rev. Lett.* **120** 123201
[40] Kozyryev I, Baum L, Matsuda K, Augenbraun B L, Anderegg L, Sedlack A P and Doyle J M 2017 Sisyphus laser cooling of a polyatomic molecule *Phys. Rev. Lett.* **118** 173201
[41] Ni K-K *et al* 2008 A high phase-space-density gas of polar molecules *Science* **322** 231
[42] Voges K K, Gersema P, Meyer zum Alten Borgloh M, Schulze T A, Hartmann T, Zenesini A and Ospelkaus S 2020 Ultracold gas of bosonic $^{23}Na^{39}K$ ground-state molecules *Phys. Rev. Lett.* **125** 083401
[43] Danzl J G, Haller E, Gustavsson M, Mark M J, Hart R, Bouloufa N, Dulieu O, Ritsch H and Nägerl H-C 2008 Quantum gas of deeply bound ground state molecules *Science* **321** 1062

[44] Danzl J G, Mark M J, Haller E, Gustavsson M, Hart R, Aldegunde J, Hutson J M and Nägerl H-C 2010 An ultracold high-density sample of rovibronic ground-state molecules in an optical lattice *Nat. Phys.* **6** 265

[45] Lang F, van der Straten P, Brandstätter B, Thalhammer G, Winkler K, Julienne P S, Grimm R and Hecker Denschlag J 2008 Cruising through molecular bound-state manifolds with radiofrequency *Nat. Phys.* **4** 223

[46] Takekoshi T, Reichsöllner L, Schindewolf A, Hutson J M, Le Sueur C R, Dulieu O, Ferlaino F, Grimm R and Nägerl H-C 2014 Ultracold dense samples of dipolar RbCs molecules in the rovibrational and hyperfine ground state *Phys. Rev. Lett.* **113** 205301

[47] Molony P K, Gregory P D, Ji Z, Lu B, Köppinger M P, Le Sueur C R, Blackley C L, Hutson J M and Cornish S L 2014 Creation of ultracold $^{87}Rb^{133}Cs$ molecules in the rovibrational ground state *Phys. Rev. Lett.* **113** 255301

[48] Park J W, Will S A and Zwierlein M W 2015 Ultracold dipolar gas of fermionic $^{23}Na^{40}K$ molecules in their absolute ground state *Phys. Rev. Lett.* **114** 205302

[49] Seeßelberg F, Buchheim N, Lu Z-K, Schneider T, Luo X-Y, Tiemann E, Bloch I and Gohle C 2018 Modeling the adiabatic creation of ultracold polar $^{23}Na^{40}K$ molecules *Phys. Rev.* A **97** 013405

[50] Yang H, Zhang D-C, Liu L, Liu Y-X, Nan J, Zhao B and Pan J-W 2019 Observation of magnetically tunable Feshbach resonances in ultracold $^{23}Na^{40}K + {}^{40}K$ collisions *Science* **363** 261

[51] Guo M *et al* 2016 Creation of an ultracold gas of ground-state dipolar $^{23}Na^{87}Rb$ molecules *Phys. Rev. Lett.* **116** 205303

[52] Rvachov T M, Son H, Sommer A T, Ebadi S, Park J J, Zwierlein M W, Ketterle W and Jamison A O 2017 Long-lived ultracold molecules with electric and magnetic dipole moments *Phys. Rev. Lett.* **119** 143001

[53] Cairncross W B, Zhang J T, Picard L R B, Yu Y, Wang K and Ni K-K 2021 Assembly of a rovibrational ground state molecule in an optical tweezer *Phys. Rev. Lett.* **126** 123402

[54] Gregory P D, Frye M D, Blackmore J A, Bridge E M, Sawant R, Hutson J M and Cornish S L 2019 Sticky collisions of ultracold RbCs molecules *Nat. Commun.* **10** 3104

[55] Idziaszek Z and Julienne P S 2010 Universal rate constants for reactive collisions of ultracold molecules *Phys. Rev. Lett.* **104** 113202

[56] Idziaszek Z, Quéméner G, Bohn J L and Julienne P S 2010 Simple quantum model of ultracold polar molecule collisions *Phys. Rev.* A **82** 020703

[57] Frye M D, Julienne P S and Hutson J M 2015 Cold atomic and molecular collisions: approaching the universal loss regime *New J. Phys.* **17** 045019

[58] Mayle M, Ruzic B P and Bohn J L 2012 Statistical aspects of ultracold resonant scattering *Phys. Rev.* A **85** 062712

[59] Mayle M, Quéméner G, Ruzic B P and Bohn J L 2013 Scattering of ultracold molecules in the highly resonant regime *Phys. Rev.* A **87** 012709

[60] Christianen A, Karman T and Groenenboom G C 2019 A quasiclassical method for calculating the density of states of ultracold collision complexes *Phys. Rev.* A **100** 032708

[61] Christianen A, Zwierlein M W, Groenenboom G C and Karman T 2019 Photoinduced two-body loss of ultracold molecules *Phys. Rev. Lett.* **123** 123402

[62] Gregory P D, Blackmore J A, Bromley S L and Cornish S L 2020 Loss of ultracold $^{87}Rb^{133}Cs$ molecules via optical excitation of long-lived two-body collision complexes *Phys. Rev. Lett.* **124** 163402

[63] Gregory P D, Blackmore J A, Frye M D, Fernley L M, Bromley S L, Hutson J M and Cornish S L 2021 Molecule–molecule and atom–molecule collisions with ultracold RbCs molecules *New J. Phys.* **23** 125004

[64] Liu Y, Hu M-G, Nichols M A, Grimes D D, Karman T, Guo H and Ni K-K 2021 Photo-excitation of long-lived transient intermediates in ultracold reactions *Nat. Phys.* **16** 1132

[65] Bause R, Schindewolf A, Tao R, Duda M, Chen X-Y, Quéméner G, Karman T, Christianen A, Bloch I, Luo X-Y *et al* 2021 Collisions of ultracold molecules in bright and dark optical dipole traps *Phys. Rev. Research* **3** 033013

[66] Gersema P, Voges K, Meyer zum Alten Borgloh M, Koch L, Hartmann T, Zenesini A, Ospelkaus S, Lin J, He J and Wang D 2021 Probing photoinduced two-body loss of ultracold non-reactive bosonic $^{23}Na^{87}Rb$ and $^{23}Na^{39}K$ molecules *Phys. Rev. Lett.* **127** 163401

[67] Nichols M A, Liu Y-X, Zhu L, Hu M-G, Liu Y and Ni K-K 2021 Detection of long-lived complexes in ultracold atom–molecule collisions (arXiv:2105.14960)

[68] Voges K K, Gersema P, Hartmann T, Ospelkaus S and Zenesini A 2021 Hyperfine dependent atom–molecule loss analyzed by the analytic solution of few-body loss equations (arXiv:2109.03605)

[69] Wang X-Y, Frye M D, Su Z, Cao J, Liu L, Zhang D-C, Yang H, Hutson J M, Zhao B, Bai C-L and Pan J-W 2021 Magnetic Feshbach resonances in collisions of $^{23}Na^{40}K$ with ^{40}K *New J. Phys.* **23** 115010

[70] Ashton C J, Child M S and Hutson J M 1983 Rotational predissociation of the Ar-HCl van der Waals complex—close-coupled scattering calculations *J. Chem. Phys.* **78** 4025

[71] Feshbach H 1958 Unified theory of nuclear reactions *Ann. Phys., NY* **5** 357

[72] Feshbach H 1962 A unified theory of nuclear reactions. II *Ann. Phys., NY* **19** 287

[73] Fano U 1961 Effects of configuration interaction on intensities and phase shifts *Phys. Rev.* **124** 1866

[74] Bohm A, Harshman N L and Walther H 2002 Relating the Lorentzian and exponential: Fermi's approximation, the Fourier transform, and causality *Phys. Rev.* A **66** 012107

[75] Mies F H and Julienne P S 1984 A multichannel quantum defect analysis of two-state couplings in diatomic molecules *J. Chem. Phys.* **80** 2526

[76] Mies F H 1984 A multichannel quantum defect analysis of diatomic predissociation and inelastic atomic scattering *J. Chem. Phys.* **80** 2514

[77] Mies F H and Raoult M 2000 Analysis of threshold effects in ultracold atomic collisions *Phys. Rev.* A **62** 012708

[78] Raoult M and Mies F H 2004 Feshbach resonance in atomic binary collisions in the Wigner threshold law regime *Phys. Rev.* A **70** 012710

[79] Gribakin G F and Flambaum V V 1993 Calculation of the scattering length in atomic collisions using the semiclassical approximation *Phys. Rev.* A **48** 546

[80] Mitchell G E, Richter A and Weidenmüller H A 2010 Random matrices and chaos in nuclear physics: nuclear reactions *Rev. Mod. Phys.* **2845–2901** 760

[81] Frye M D and Hutson J M 2019 Time delays in ultracold atomic and molecular collisions *Phys. Rev. Res.* **1** 033023

[82] Croft J F E, Bohn J L and Quéméner G 2020 Unified model of ultracold molecular collisions *Phys. Rev.* A **102** 033306

[83] Christianen A, Groenenboom G C and Karman T 2021 Lossy quantum defect theory of ultracold molecular collisions *Phys. Rev.* A **104** 043327

[84] Żuchowski P S and Hutson J M 2010 Reactions of ultracold alkali metal dimers *Phys. Rev.* A **81** 060703(R)
[85] Żuchowski P S, Kosicki M, Kodrycka M and Soldán P 2013 van der Waals coefficients for systems with ultracold polar alkali-metal molecules *Phys. Rev.* A **87** 022706
[86] Derevianko A, Porsev S G and Babb J F 2010 Electric dipole polarizabilities at imaginary frequencies for the alkali-metal, alkaline-earth, and inert gas atoms *At. Data Nucl. Data Tables* **96** 323
[87] Linton C, Martin F, Ross A J, Russier I, Crozet P, Yiannopoulou A, Li L and Lyyra A M 1999 The high-lying vibrational levels and dissociation energy of the $a^3\Sigma_u^+$ state of $^7Li_2$ *J. Mol. Spectrosc.* **196** 20
[88] Amiot C and Dulieu O 2002 The Cs_2 ground electronic state by Fourier transform spectroscopy: dispersion coefficients *J. Chem. Phys.* **117** 5155
[89] Pashov A, Docenko O, Tamanis M, Ferber R, Knöckel H and Tiemann E 2005 Potentials for modeling cold collisions between Na (3s) and Rb (5s) atoms *Phys. Rev.* A **72** 062505
[90] Coxon J A and Melville T C 2006 Application of direct potential fitting to line position data for the $X^1\Sigma_g^+$ and $A^1\Sigma_u^+$ states of Li_2 *J. Mol. Spectrosc.* **235** 235
[91] Docenko O, Tamanis M, Zaharova J, Ferber R, Pashov A, Knöckel H and Tiemann E 2006 The coupling of the $X^1\Sigma^+$ and $a^3\Sigma^+$ states of the atom pair Na plus Cs and modelling cold collisions *J. Phys. B: At. Mol. Opt. Phys.* **39** S929
[92] Staanum P, Pashov A, Knöckel H and Tiemann E 2007 $X^1\Sigma^+$ and $a^3\Sigma^+$ states of LiCs studied by Fourier-transform spectroscopy *Phys. Rev.* A **75** 042513
[93] Pashov A, Docenko O, Tamanis M, Ferber R, Knöckel H and Tiemann E 2007 Coupling of the $X^1\Sigma^+$ and $a^3\Sigma^+$ states of KRb *Phys. Rev.* A **76** 022511
[94] Gerdes A, Hobein M, Knöckel H and Tiemann E 2008 Ground state potentials of the NaK molecule *Eur. Phys. J.* D **49** 67
[95] Falke S, Knöckel H, Friebe J, Riedmann M, Tiemann E and Lisdat C 2008 Potassium ground-state scattering parameters and Born–Oppenheimer potentials from molecular spectroscopy *Phys. Rev.* A **78** 012503
[96] Tiemann E, Knöckel H, Kowalczyk P, Jastrzebski W, Pashov A, Salami H and Ross A J 2009 Coupled system $a^3\Sigma^+$ and $X^1\Sigma^+$ of KLi: Feshbach resonances and corrections to the Born–Oppenheimer approximation *Phys. Rev.* A **79** 042716
[97] Strauss C, Takekoshi T, Lang F, Winkler K, Grimm R, Hecker Denschlag J and Tiemann E 2010 Hyperfine, rotational, and vibrational structure of the $a^3\Sigma_u^+$ state of $^{87}Rb_2$ *Phys. Rev.* A **82** 052514
[98] Ivanova M, Stein A, Pashov A, Knöckel H and Tiemann E 2011 The $X^1\Sigma^+$ state of LiRb studied by Fourier-transform spectroscopy *J. Chem. Phys.* **134** 024321
[99] Knoop S, Schuster T, Scelle R, Trautmann A, Appmeier J, Oberthaler M K, Tiesinga E and Tiemann E 2011 Feshbach spectroscopy and analysis of the interaction potentials of ultracold sodium *Phys. Rev.* A **83** 042704
[100] Docenko O, Tamanis M, Ferber R, Knöckel H and Tiemann E 2011 Singlet and triplet potentials of the ground state atom pair Rb + Cs studied by Fourier-transform spectroscopy *Phys. Rev.* A **83** 052519
[101] Takekoshi T *et al* 2012 Towards the production of ultracold ground-state RbCs molecules: Feshbach resonances, weakly bound states, and coupled-channel models *Phys. Rev.* A **85** 032506
[102] Steinke M, Knöckel H and Tiemann E 2012 $(X)1\,^1\Sigma^+$ state of LiNa studied by Fourier-transform spectroscopy *Phys. Rev.* A **85** 042720
[103] Schuster T, Scelle R, Trautmann A, Knoop S, Oberthaler M K, Haverhals M M, Goosen M R, Kokkelmans S J J M F and Tiemann E 2012 Feshbach spectroscopy and scattering properties of ultracold Li + Na mixtures *Phys. Rev.* A **85** 042721
[104] Wang F, Xiong D, Li X, Wang D and Tiemann E 2013 Observation of Feshbach resonances between ultracold Na and Rb atoms *Phys. Rev.* A **87** 050702(R)
[105] Repp M, Pires R, Ulmanis J, Heck R, Kuhnle E D, Weidemüller M and Tiemann E 2013 Observation of interspecies ^{6}Li-^{133}Cs Feshbach resonances *Phys. Rev.* A **87** 010701
[106] Ferber R, Nikolayeva O, Tamanis M, Knöckel H and Tiemann E 2013 Long-range coupling of $X^1\Sigma^+$ and $a^3\Sigma^+$ states of the atom pair K + Cs *Phys. Rev.* A **88** 012516
[107] Julienne P S and Hutson J M 2014 Contrasting the wide Feshbach resonances in ^{6}Li and ^{7}Li *Phys. Rev.* A **89** 052715
[108] Maier R A W, Eisele M, Tiemann E and Zimmermann C 2015 Efimov resonance and three-body parameter in a lithium–rubidium mixture *Phys. Rev. Lett.* **1152** 043201
[109] Zhu M-J *et al* 2017 Feshbach loss spectroscopy in an ultracold ^{23}Na–^{40}K mixture *Phys. Rev.* A **96** 062705
[110] Gröbner M, Weinmann P, Kirilov E, Nägerl H-C, Julienne P S, Le Sueur C R and Hutson J M 2017 Observation of interspecies Feshbach resonances in an ultracold ^{39}K-^{133}Cs mixture and refinement of interaction potentials *Phys. Rev.* A **95** 022715
[111] Sovkov V B, Xie F, Lyyra A M, Ahmed E H, Ma J and Jia S 2017 Re-examination of the Cs_2 ground singlet $X^1\Sigma_g^+$ and triplet $a^3\Sigma_u^+$ states *J. Chem. Phys.* **147** 104301
[112] Hartmann T, Schulze T A, Voges K K, Gersema P, Gempel M W, Tiemann E, Zenesini A and Ospelkaus S 2019 Feshbach resonances in ^{23}Na + ^{39}K mixtures and refined molecular potentials for the NaK molecule *Phys. Rev.* A **99** 032711
[113] Tiemann E, Gersema P, Voges K K, Hartmann T, Zenesini A and Ospelkaus S 2020 Beyond Born–Oppenheimer approximation in ultracold atomic collisions *Phys. Rev. Res.* **2** 013366
[114] Guo Z, Jia F, Zhu B, Li L, Hutson J M and Wang D 2021 Tunable Feshbach resonances and interaction potentials between ^{23}Na and ^{87}Rb atoms (arXiv:2108.01856)
[115] Martins J L, Car R and Buttet J 1983 Electronic properties of alkali trimers *J. Chem. Phys.* **78** 5646
[116] Lindsay D M and Thompson G A 1982 Dynamic frequency shifts in pseudorotating Na_3 *J. Chem. Phys.* **77** 1114
[117] Thompson G A and Lindsay D M 1981 ESR spectra of matrix isolated potassium atom clusters *J. Chem. Phys.* **74** 959
[118] Garland D A and Lindsay D M 1983 Electron-spin resonance of pseudorotating $^6Li_3$ and $^7Li_3$ clusters *J. Chem. Phys.* **78** 2813
[119] Mile B, Rowlands C C, Sillman P D and Yacob A R 1995 The EPR spectrum and structure of the mixed alkali metal trimer cluster Na_2Li prepared using a rotating cryostat *J. Chem. Soc., Chem. Commun.* 775–6
[120] Hishinuma N 1995 Observation of molecular-beam magnetic resonance of Li_3 clusters *Phys. Rev.* A **46** 7023
[121] Coudert L H, Ernst W E and Golonzka O 2002 Hyperfine coupling and pseudorotational motion interaction in Na_3 *J. Chem. Phys.* **117** 7102
[122] Hauser A W, Pototschnig J V and Ernst W E 2015 A classic case of Jahn–Teller effect theory revisited: *ab initio* simulation of hyperfine coupling and pseudorotation in the $1^2E'$ state of Na_3 *Chem. Phys.* **460** 2
[123] London F 1929 Quantenmechanische Deutung des Vorgangs der Aktivierung *Z. Electrochem.* **35** 552
[124] Eyring H and Polanyi M 1930 Zur Berechnung der Aktivierungswärme *Naturwissenschaften* **18** 914
[125] Sato S 1955 On a new method of drawing the potential energy surface *J. Chem. Phys.* **23** 592

[126] Truhlar D G and Wyatt R E 1977 H + H_2: Potential-Energy Surfaces and Elastic and Inelastic Scattering *Advances in Chemical Physics* vol 36 ed I Prigogine and S A Rice (New York: Wiley) pp 141–204
[127] Varandas A J C and Morais V M F 1982 Semi-empirical valence bond potential energy surfaces for homonuclear alkali trimers *Mol. Phys.* **47** 1241
[128] Varandas A J C, Morais V M F and Pais A A C C 1986 Semiempirical valence bond potential energy surfaces for the alkali trimers *Mol. Phys.* **58** 285
[129] Slater J C 1931 Molecular energy levels and valence bonds *Phys. Rev.* **38** 1109
[130] Harney H L, Richter A and Weidenmüller H A 1986 Breaking of isospin symmetry in compound-nucleus reactions *Rev. Mod. Phys.* **58** 607
[131] Mehta M L 1991 *Random Matrices* 2nd edn (New York: Academic)
[132] Guhr T, Müller–Groeling A and Weidenmüller H A 1998 Random-matrix theories in quantum physics: common concepts *Phys. Rep.* **299** 9
[133] Aldegunde J and Hutson J M 2017 Hyperfine structure of alkali-metal diatomic molecules *Phys. Rev.* A **96** 042506
[134] Hutson J M 2007 Feshbach resonances in ultracold atomic and molecular collisions: threshold behaviour and suppression of poles in scattering lengths *New J. Phys.* **9** 152
[135] Gao B 1998 Solutions of the Schrödinger equation for an attractive $1/r^6$ potential *Phys. Rev.* A **58** 1728
[136] Julienne P S and Gao B 2006 Simple theoretical models for resonant cold atom interactions *AIP Conf. Proc.* **869** 261